Supplementary Information (SI) for Journal of Materials Chemistry C.

Supporting Information

Highly Linearly Polarized CdSe/CdS/ZnS Nanoplatelets-Assembled Microsphere Laser

Yuan Jiang[la,b], Linqi Chen[l*a], Hongyu Yang[lc], Jingzhou Li*[d], Xuting Chen[a,b], Xinjie Li[a,b], Hongxing Dong*[a], Long Zhang[e]

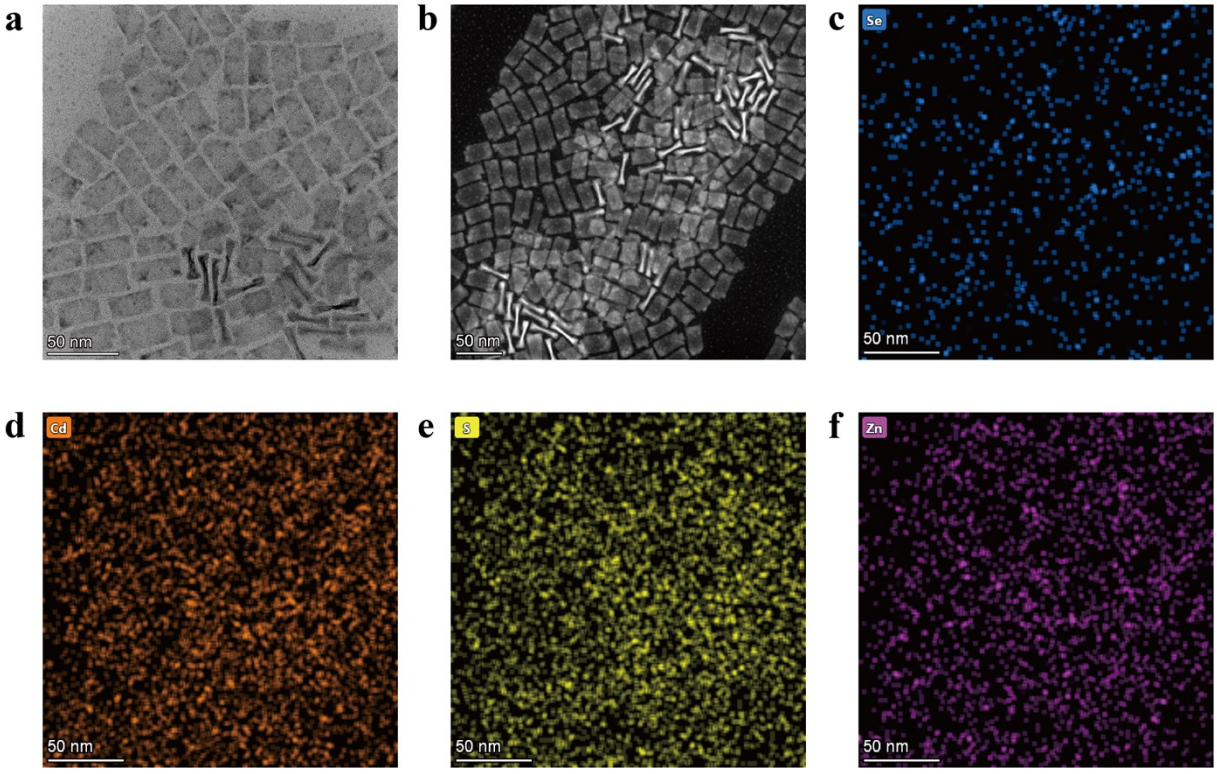

Figure S1. (a) TEM images of CdSe/CdS/ZnS NPLs. (b) High-angle annual dark-field scanning transmission electron microscopy (HAADF-STEM) image of CdSe/CdS/ZnS NPLs and (c-f) their high-resolution elemental mapping.

Table S1. Energy dispersive X-ray spectroscopy (EDS) results of the CdSe/CdS/ZnS nanoplatelets.

Z	Element	Family	Atomic Fraction (%)	Atomic Error (%)	Mass Fraction (%)	Mass Error (%)	Mass Error (%)
16	S	K	50.40	4.84	27.13	1.69	0.85
30	Zn	K	23.56	3.86	25.87	3.79	0.76
34	Se	K	3.76	0.63	4.99	0.74	4.24
48	Cd	L	22.27	3.34	42.02	5.50	0.70

Table S2. XPS compositional analysis of the CdSe/CdS/ZnS nanoplatelets.

	Peak	**Binding Energy(ev)**	**FWHM**	**Area**	**%Conc.**
C	C 1s A	284.80	1.37	61571.16	
	C 1s B	287.99	1.97	2160.50	
Se	Se 3d5/2	53.71	1.71	1541.22	
	Se 3d3/2	54.31	1.71	1054.18	
Cd	Cd 3d5/2 A	404.42	1.02	40113.13	48.93
	Cd 3d3/2 A	411.13	1.09	26015.83	
	Cd 3d5/2 B	404.85	1.06	40424.82	51.07
	Cd 3d3/2 B	411.85	1.05	28223.37	
S	S 2p3/2 A	159.38	2.44	2762.03	13.35
	S 2p1/2 A	160.48	2.42	1407.37	
	S 2p3/2 B	161.31	1.39	17880.66	86.65
	S 2p1/2 B	162.50	1.39	9133.64	
Zn	Zn 2p3/2	1021.69	1.56	129218.58	
	Zn 2p1/2	1044.68	1.56	46919.81	

Table S3. XPS determined bulk elemental composition of the CdSe/CdS/ZnS nanoplatelets.

Element	Se%	Cd%	S%	Zn%	Cd/Se ratio	S/Zn ratio
%Conc.	4.45	15.51	47.21	32.83	3.48	1.4

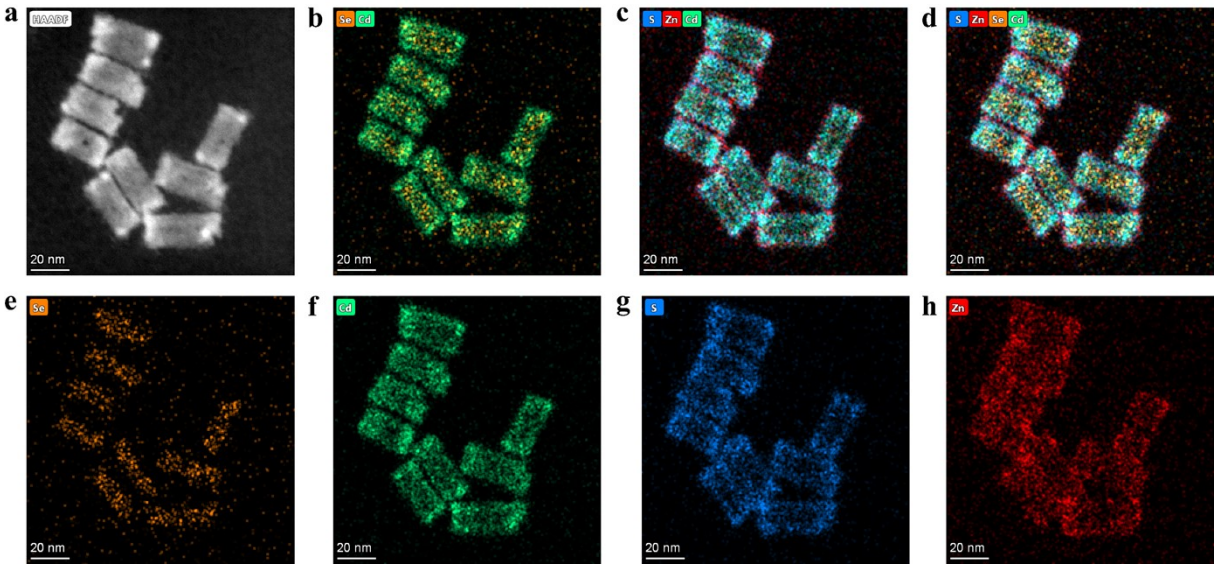

Figure S2. (a) HAADF-STEM image of core/shell NPLs and their high-resolution elemental mapping (b−h).

Component analysis of the nanoplatelets

X-ray photoelectron spectroscopy (XPS) is a commonly used technique to obtain surface compositional information of solid materials. The basic principle of this technique is to measure the binding energy of electrons emitted from the material's surface, which allows for the identification of the difference in binding energies between surface atoms and bulk atoms. Surface atoms generally have slightly higher binding energies than their corresponding bulk atoms. By analyzing the characteristic peaks of various elements in the XPS spectra, the presence and chemical state of elements in the material can be confirmed. In this study, typical characteristic peaks were observed through XPS analysis, including the Cd 3d 5/2 and 3/2, Se 3d 5/2 and 3/2, S 2p 3/2 and 1/2, and Zn 2p 3/2 and 1/2 peaks. These peaks correspond to the presence of Cd^{2+}, S^{2-}, Se^{2-}, and Zn^{2+} ions. By analyzing the positions and shapes of these peaks, it was confirmed that Cd^{2+}, S^{2-}, Se^{2-}, and Zn^{2+} elements were present in the sample, indicating the presence of CdSe, CdS, and ZnS components.

Further, XPS data revealed changes in the binding energy of Cd 3d. In CdS, the binding energy of Cd 3d is higher compared to that in CdSe materials. This suggests that the chemical environment of Cd in CdS and CdSe is different. Notably, a shift occurred in the position of the S 2p peak, with the binding energy of S 2p in ZnS moving to a higher value compared to CdS. This change may be related to the structure and chemical state of the ZnS shell, indicating that the electronic environment of the ZnS layer differs from that of the CdS layer. Additionally, the high-resolution XPS spectra are consistent with existing literature data, further confirming the presence of the CdSe/CdS/CdS composite structure. These spectra provide detailed information about the chemical states of Cd, S, Se, and Zn, which helps to better understand the surface and interfacial characteristics of this multilayer composite structure, as well as the interactions between different material layers.

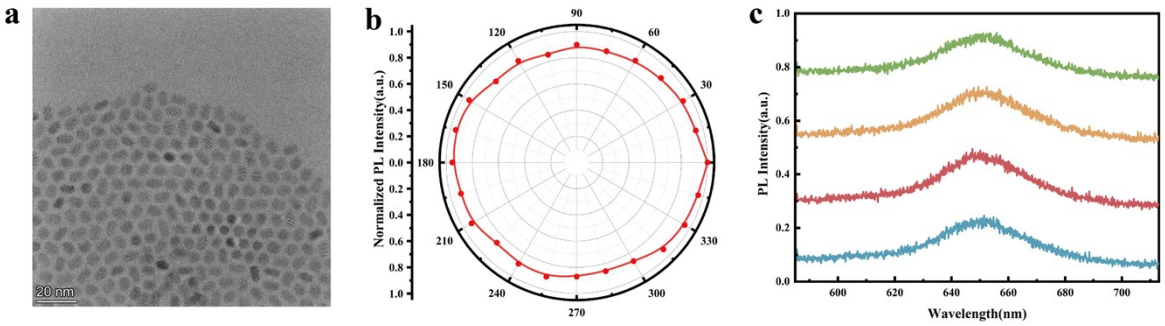

Figure S3. (a) TEM images of spherical quantum dots. (b) Full angular polarization diagram of fluorescence emission from the quantum dots. (c) Emission spectrum from the quantum dots recorded under various polarizer rotation angles. When the polarization angle θ = 0°, the photoluminescence intensity reaches its maximum, and the intensity changes little with the angle. The corresponding degree of polarization (DOP) value is 0.08. Compared to anisotropic nanoplatelets, the degree of polarization of spherical quantum dots is significantly reduced. We synthesized spherical quantum dots following a previously published procedure.

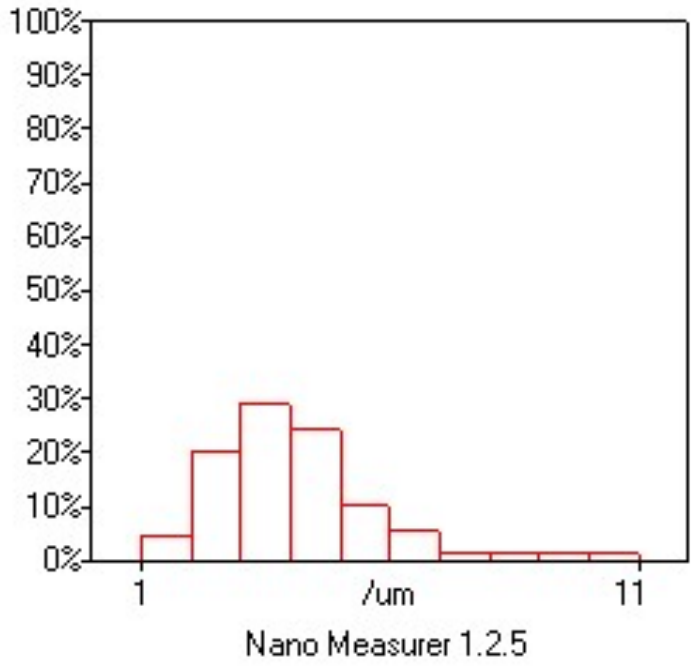

Figure S4. Histogram of microsphere diameters obtained from SEM analysis. The particle size distribution ranges from 1 to 11 μm, with a mean diameter of 2 to 4 μm.

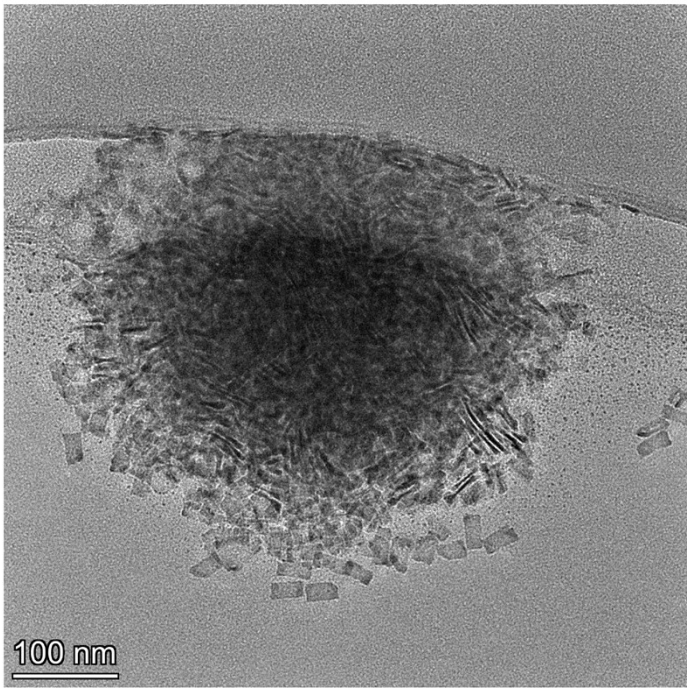

Figure S5. TEM image of the CdSe/CdS/ZnS nanoplatelets-assembled microsphere in the assembly process.

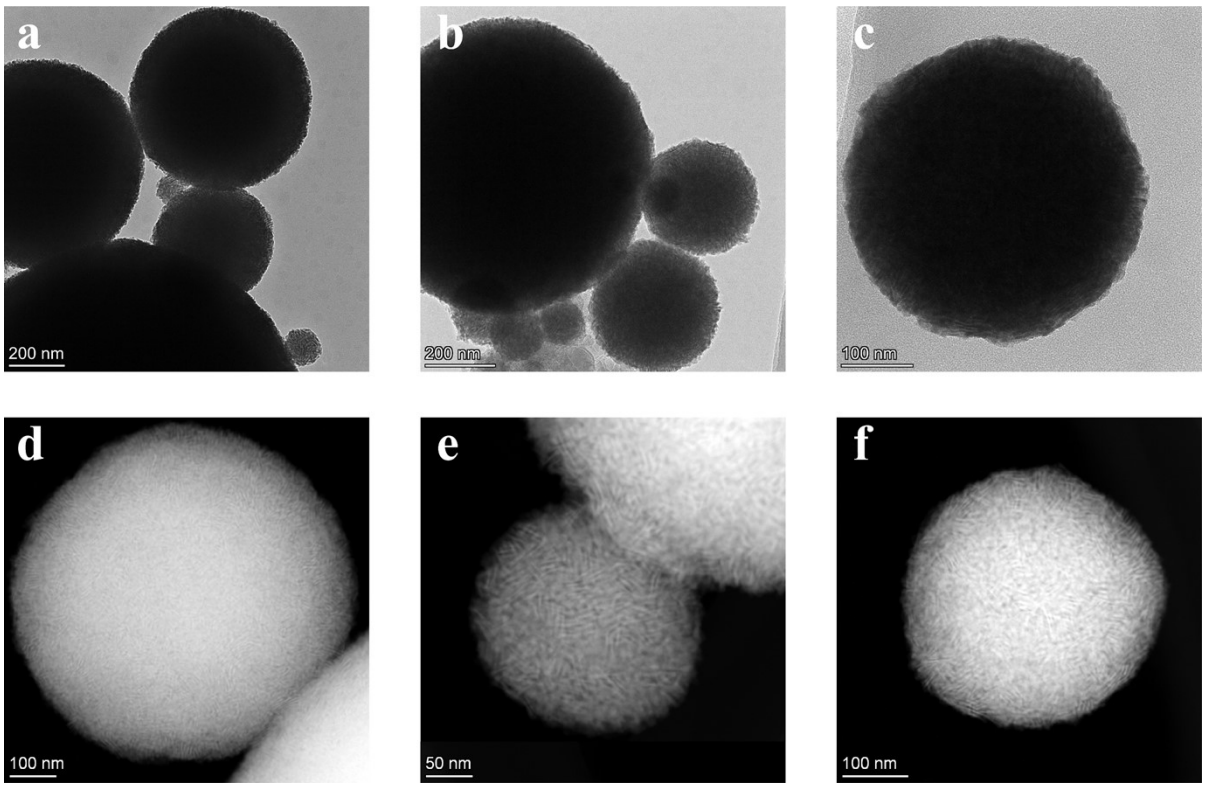

Figure S6. (a-c) TEM images of the CdSe/CdS/ZnS nanoplatelets-assembled microsphere assembled for 2–3 days. (d-f) The HAADF-STEM image of the nanoplatelets-assembled microsphere. The microspheres have good sphericity, and from the stripe dark fringes, it can be observed that the nanoplatelets inside the microspheres are arranged with their edges facing upward.

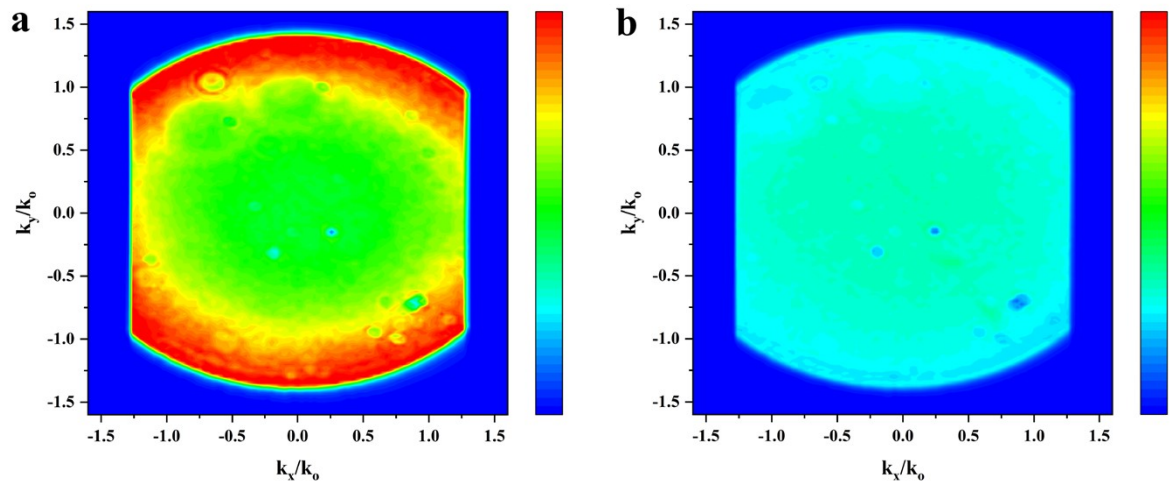

Figure S7. (a)Experimental BFP image from the CdSe/CdS/ZnS nanoplatelets-assembled microsphere. (b) Experimental BFP image from the CdSe/CdS/ZnS nanoplatelets. The back focal plane imaging involves inserting a lens, known as a Bertrand lens, into the imaging process. Back focal plane imaging involves inserting a lens known as the Bertrand lens during the imaging process. The Bertrand lens focuses on the back focal plane of the first lens, which is the objective lens. The combination of this lens and the imaging lens effectively forms an image of the back focal plane of the objective lens. The real image in the back focal plane corresponds to the Fourier transform of the parallel light emitted from the front focal plane. Therefore, the back focal plane is often referred to as the Fourier plane. Each actual image point in the back focal plane corresponds to the sum of parallel light rays emitted from a specific direction in the front focal plane. As a result, every point in the back focal plane image represents the Fourier transform of the parallel light from a specific direction in the front focal plane. By measuring the angular distribution of light in the back focal plane image, the orientation of nanoplatelets in the sample can be inferred.

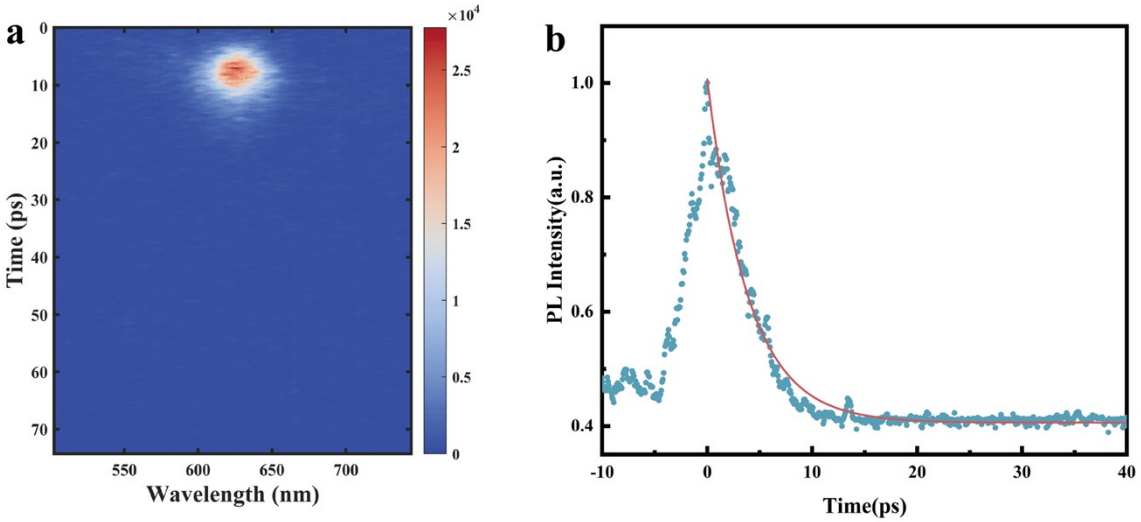

Figure S8. (a) Single-mode laser streak camera imaging of CdSe/CdS/ZnS nanoplatelets-assembled microsphere microspheres. (b) TRPL decay curves of CdSe/CdS/ZnS nanoplatelets-assembled microsphere for single-mode laser.

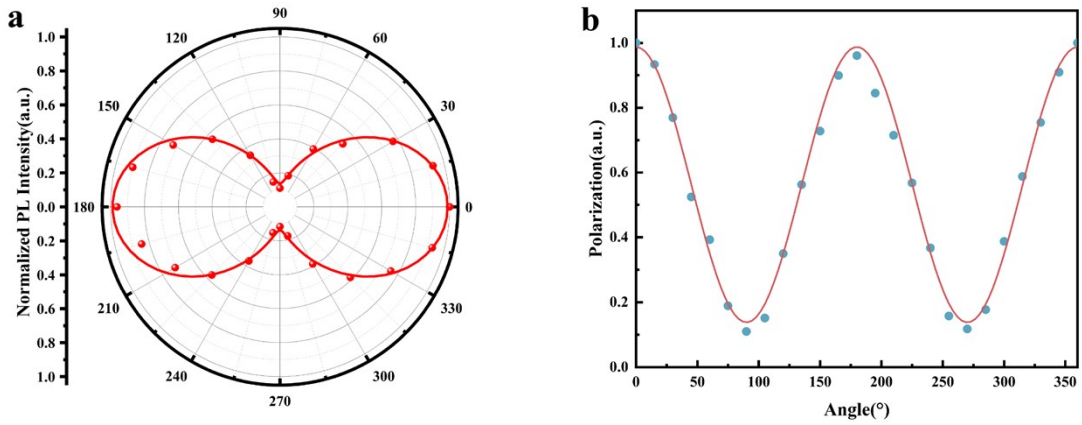

Figure S9. (a) Full angular polarization diagram of lasing from the CdSe/CdS/ZnS nanoplatelets-assembled microsphere. (b) The modified Malus' law fitting of polarization degree of the CdSe/CdS/ZnS nanoplatelets-assembled microsphere, the red curve is the fitted curve, and the blue point is the measured degree of polarization. According to the modified Malus' law, the intensity passing through the polarizer follows the relationship, and thus the polarization graph can be fitted with the equation:

$I = (I_o P) COS^2(\theta) + I_{bg}$

Where, I_o is the initial light intensity of the source, P is the degree of polarization of the light source ($0 \leq P \leq 1$); if the light source is completely polarized, then P=1, θ is the angle between the incident light polarization direction and the polarization axis of the polarizer, I_{bg} is the background light intensity, which is caused by ambient light or stray light from experimental equipment. The results obtained from the measurements are in good agreement with the fitting based on the above formula. The fitting yields a linear polarization degree of 0.89 for the nanoplatelets-assembled microsphere.

Reference

1 R. Scott, J. Heckmann, A. V. Prudnikau, A. Antanovich, A. Mikhailov, N. Owschimikow, M. Artemyev, J. I. Climente, U. Woggon, N. B. Grosse and A. W. Achtstein, *Nature Nanotech*, 2017, **12**, 1155–1160.

2 Y. Zeng, W. Yu, Y. Liu, W. Chen, Q. Wang, F. Cao, J. Wei, F. Liu, X. Yang and H. Li, *Advanced Materials*, 2025, **37**, 2415569.

3 L. Wang, M. Niu and Z. Wu, *Current Applied Physics*, 2009, **9**, 1112–1116.

4 G. Zorn, S. R. Dave, X. Gao and D. G. Castner, *Anal. Chem.*, 2011, **83**, 866–873.

5 D. U. Lee, D. H. Kim, D. H. Choi, S. W. Kim, H. S. Lee, K.-H. Yoo and T. W. Kim, *Opt. Express, OE*, 2016, **24**, A350–A357.

6 K. L. Sowers, Z. Hou, J. J. Peterson, B. Swartz, S. Pal, O. Prezhdo and T. D. Krauss, *Chemical Physics*, 2016, **471**, 24–31.

7 C. E. Rowland, I. Fedin, H. Zhang, S. K. Gray, A. O. Govorov, D. V. Talapin and R. D. Schaller, *Nature Mater*, 2015, **14**, 484–489.

8 P. Bai, A. Hu, Y. Liu, Y. Jin and Y. Gao, *J. Phys. Chem. Lett.*, 2020, **11**, 4524–4529.

9 D. A. Hanifi, N. D. Bronstein, B. A. Koscher, Z. Nett, J. K. Swabeck, K. Takano, A. M. Schwartzberg, L. Maserati, K. Vandewal, Y. Van De Burgt, A. Salleo and A. P. Alivisatos, *Science*, 2019, **363**, 1199–1202.

10 C. Liao, R. Xu, Y. Xu, C. Zhang, M. Xiao, L. Zhang, C. Lu, Y. Cui and J. Zhang, *J. Phys. Chem. Lett.*, 2016, **7**, 4968–4976.

11 N. F. Hartmann, M. Otten, I. Fedin, D. Talapin, M. Cygorek, P. Hawrylak, M. Korkusinski, S. Gray, A. Hartschuh and X. Ma, *Nat Commun*, 2019, **10**, 3253.